Matrix analysis of high-density arrayed waveguides: Crosstalk suppression by bending

Panu Hildén[*] and Andriy Shevchenko

Department of Applied Physics, Aalto University, P.O. Box 13500, Aalto FI-00076, Finland

For many photonic devices, crosstalk between densely packed waveguides poses a major problem leading to unreliable or inefficient operation of the device. In this work, a general method for modeling the crosstalk, not only in straight waveguide arrays but also in curved ones, is introduced. The method is based on a matrix analysis of electromagnetic field coupling between closely spaced waveguides. As an example, we show how bending of waveguides in an array reduces the crosstalk. The approach can help overcome the crosstalk problem in a variety of photonic integrated devices, including phased waveguide arrays, arrayed waveguide gratings, optical multiplexers, and high-density interconnects between optical and electronic components.

I. INTRODUCTION

Photonic integrated circuits are transforming many areas of science and technology by increasing the reliance on optical, rather than electrical, signals, which offer high bandwidths alongside a low energy consumption [1–3]. In practice, silicon micro- and nanostructures provide the most convenient platform for such circuits, because they are essentially lossless in the infrared spectral range and their fabrication processes are well developed in the CMOS industry [1–4]. However, the relatively long wavelengths of light limit the miniaturization of photonic chips, since a subwavelength distance between waveguides leads to significant optical coupling between them [5]. Control of this coupling, usually called the crosstalk, is a crucial part of the design of photonic integrated circuits.

Densely packed waveguides are routinely bent when connecting optical components in photonic integrated circuits. In addition, closely spaced bent waveguides can themselves be functional parts of these components, e.g., in folded microring resonators [6] or pressure sensors [7]. Most notably, bent waveguide arrays are used as arrayed waveguide gratings and phased arrays [8–10] in applications such as wavelength-division multiplexing for optical communications [9,11] and beam steering in LIDARs [12,13]. For such applications, the dense packaging of waveguides is important not only for minimizing the footprint of the device but also for preventing the appearance of multiple diffraction orders, especially in LIDAR scanners.

The design of arrayed waveguides often relies on analytical models for light propagation, e.g., to evaluate the crosstalk between the waveguides [14–18] or optical losses and intermodal coupling caused by waveguide bending [19–23]. These models can help one to develop methods for reducing the crosstalk [24–26] and improving the performance of bent waveguides [27–29]. One of the methods, inspired by the structure of compound eyes of insects, is based on blocking the light between the waveguides with an absorbing material (filled with a pigment in the case of insects) [30,31]. Recently, there has been growing interest in suppressing the crosstalk in bent waveguide arrays [32–35]. However, while the crosstalk reduction has been considered previously, e.g., in a sinusoidally curved waveguide coupler [36] and in superlattices [37], an analytical model treating the crosstalk in bent arrays with an arbitrary number of waveguides appears to be missing from the existing scientific literature.

In this work, we introduce a general matrix-based approach to analyze the propagation of light in straight or bent waveguide arrays. The approach makes it possible to represent the fields propagating in an array as superpositions of the eigenmodes of the array or the modes of the individual waveguides (cf. Refs. [14,17,21]). The field propagation and the crosstalk can then be studied using the transformation between the two representations, in a manner analogous to using Fourier optics to solve diffraction problems. The analysis results in several notable findings. We observe that the eigenmodes of a significantly bent waveguide array are concentrated in one or a few

---

[*]Contact author: panu.hilden@aalto.fi

waveguides. During the propagation, light oscillates back and forth between the original waveguide and its neighbors in a periodic manner. This behavior is similar to optical Bloch oscillation, which is a consequence of equidistant spacing of the propagation constants in neighboring waveguides [38,39]. We find that by matching the length of the waveguide array with the beating period, the crosstalk can be suppressed in waveguide arrays with rather large radii of curvature. The presented analysis not only helps to explain the details of the crosstalk phenomenon but also offers efficient analytical tools for assessing the crosstalk in both straight and bent waveguides without the need for computationally expensive three-dimensional simulations.

The paper is organized as follows. In Sec. II, we introduce a matrix description of the light propagation in straight waveguide arrays. In Sec. III, the approach is generalized to also be applicable to bent waveguide arrays. Section IV is focused on the crosstalk dynamics in bent and straight waveguide arrays. The conclusions of this work are drawn in Sec. V.

II. MODE-TRANSFORMATION MATRICES FOR AN ARRAY OF STRAIGHT WAVEGUIDES

The eigenmodes of a waveguide array, which we call supermodes, are invariant with respect to their propagation in the array, except for a phase $\phi = \beta z$ determined by the mode propagation constant β and distance z. The propagation invariance makes the supermodes form a convenient basis for modeling the crosstalk. For straight waveguides, the field profiles and propagation constants of the supermodes, denoted, respectively, by $\tilde{\mathbf{e}}_j$ and β_j for a jth supermode, are relatively easy to calculate, e.g., numerically. Here, the electric and magnetic fields, denoted by the lowercase letters $\mathbf{e}$ and $\mathbf{h}$, are normalized such that

$$\frac{1}{2} \iint_{-\infty}^{\infty} \mathrm{Re}\{\mathbf{e}^* \times \mathbf{h}\} \cdot \hat{\mathbf{z}} \, dx \, dy = 1, \qquad (1)$$

where x and y are the transverse coordinates and $\hat{\mathbf{z}}$ is the unit vector along the z axis. In this work, we use the
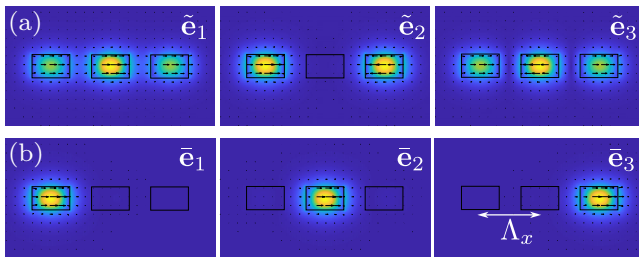

FIG. 1. (a) The TE supermodes $\tilde{\mathbf{e}}_1$, $\tilde{\mathbf{e}}_2$, and $\tilde{\mathbf{e}}_3$ of a straight waveguide array. (b) The corresponding TE modes of the individual waveguides.

COMSOL MULTIPHYSICS software (the mode-analysis eigenvalue solver of the wave-optics module) to find the supermodes of particular waveguide arrays. For example, in Fig. 1(a) we show the transverse-electric (TE) supermodes of an array of three single-mode silicon waveguides embedded in glass. Each waveguide is 300 nm high and 500 nm wide. The period of the array is $\Lambda_x = 800$ nm. The mode wavelength is 1550 nm. These four parameters will be retained for all the waveguide arrays of this type considered in this work. Both silicon and glass are highly transparent at this wavelength. Their refractive indices are 3.48 and 1.44, respectively.

An arbitrary electric field $\mathbf{E}$ propagating in an array of N waveguides can be expressed as a superposition of the normalized supermodes:

$$\mathbf{E} = \tilde{\mathbf{a}}\tilde{\mathbf{E}} = \sum_{j=1}^{N} \begin{bmatrix} \tilde{a}_j \tilde{e}_{xj} & \tilde{a}_j \tilde{e}_{yj} & \tilde{a}_j \tilde{e}_{zj} \end{bmatrix}. \qquad (2)$$

Here, the elements of N-dimensional vector $\tilde{\mathbf{a}} = [\tilde{a}_1 \ \tilde{a}_2 \ \cdots \ \tilde{a}_N]$ are the complex amplitudes of the supermodes, whereas $\tilde{\mathbf{E}} = [\tilde{\mathbf{e}}_1 \ \tilde{\mathbf{e}}_2 \ \cdots \ \tilde{\mathbf{e}}_N]^T$ is an $N \times 3$ matrix, the row vectors of which are the supermode fields expressed through their Cartesian components. Note that the number of supermodes is the same as the number of waveguides in the system, since this is the number of complex amplitudes of the modes needed to describe an arbitrary propagating field in the array. The complex amplitudes of the supermodes change upon propagation in accordance with the expression

$$\tilde{\mathbf{a}}(z) = \tilde{\mathbf{g}}(z) \circ \tilde{\mathbf{a}}(0), \qquad (3)$$

where "$\circ$" denotes the Hadamard product and $\tilde{\mathbf{g}}(z) = \exp(i\boldsymbol{\beta}z)$ is the transfer function vector; vector $\boldsymbol{\beta} = [\beta_1 \ \beta_2 \ \cdots \ \beta_N]$ contains the propagation constants of the supermodes. With this in mind, any change in $\mathbf{E}$ as a function of z, including the crosstalk, can be understood as a consequence of the change in the interference pattern of the supermodes dictated by the difference in their propagation constants β_j. Now, if $\mathbf{E}(0)$ represents the field in a single waveguide of the array at $z = 0$, $\mathbf{E}(z)$ will be the field in the array at any propagation distance z, automatically showing optical coupling between the waveguides, i.e., the crosstalk. In the following, we also represent $\mathbf{E}$ in terms of the fields propagating in each individual waveguide of the array.

Suppose that $\bar{\mathbf{e}}(x, y)$ is the field distribution of an eigenmode of a single waveguide. Then, the field $\mathbf{E}$ can be expressed as a superposition of the fields of the form $\bar{\mathbf{e}}_i = \bar{\mathbf{e}}(x - x_i, y)$, where $x_i = \Lambda_x(i - \langle i \rangle)$ is the x coordinate at the center of the ith waveguide, while the origin $x = 0$ is at the center of the waveguide array. Here, $\langle i \rangle = (N + 1)/2$ is the average value of index i for a given array. The influence of the neighboring waveguides on the mode profile is

usually relatively small and we neglect it here for simplicity. The single-waveguide modes that are the counterparts to the supermodes in Fig. 1(a) are shown in Fig. 1(b). The supermodes can be represented as coherent superpositions of the single-waveguide modes as follows:

$$\tilde{\mathbf{e}}_j = \tilde{\tilde{\mathbf{c}}}_j \bar{\mathbf{E}}, \tag{4}$$

where $\bar{\mathbf{E}} = [\bar{\mathbf{e}}_1 \ \bar{\mathbf{e}}_2 \ \cdots \ \bar{\mathbf{e}}_N]^T$ is a matrix composed of the fields of single-waveguide modes and $\tilde{\tilde{\mathbf{c}}}_j$ is a normalized vector ($\|\tilde{\tilde{\mathbf{c}}}_j\| = 1$), the elements of which are the expansion coefficients of the jth supermode. Each expansion coefficient $\tilde{\tilde{c}}_{ji}$ in vector $\tilde{\tilde{\mathbf{c}}}_j$ describes the contribution of the field in the ith waveguide to the total field of the jth supermode and is given by the overlap integral [15],

$$\begin{aligned}\tilde{\tilde{c}}_{ji} &= c(\tilde{\mathbf{e}}_j, \tilde{\mathbf{h}}_j, \bar{\mathbf{e}}_i, \bar{\mathbf{h}}_i) \\ &= \frac{1}{4} \iint_{-\infty}^{\infty} \left(\tilde{\mathbf{e}}_j^* \times \bar{\mathbf{h}}_i + \bar{\mathbf{e}}_i \times \tilde{\mathbf{h}}_j^* \right) \cdot \hat{\mathbf{z}} \, dx \, dy.\end{aligned} \tag{5}$$

Collecting the expansion coefficients in a matrix,

$$\tilde{\tilde{\mathbf{C}}} = \begin{bmatrix} \tilde{\tilde{c}}_{11} & \tilde{\tilde{c}}_{12} & \cdots & \tilde{\tilde{c}}_{1N} \\ \tilde{\tilde{c}}_{21} & \tilde{\tilde{c}}_{22} & & \\ \vdots & & \ddots & \\ \tilde{\tilde{c}}_{N1} & & & \tilde{\tilde{c}}_{NN} \end{bmatrix}, \tag{6}$$

we obtain the representation connecting the supermodes with the single-waveguide modes. For the expansion coefficients of any given field in the two representations, we have

$$\tilde{\mathbf{E}} = \tilde{\tilde{\mathbf{C}}}\bar{\mathbf{E}}, \tag{7}$$

$$\tilde{\mathbf{a}}^T = \tilde{\tilde{\mathbf{C}}}\bar{\mathbf{a}}^T. \tag{8}$$

If the coupling between the waveguides that are not immediate neighbors is negligible, the expansion coefficients take the form $\tilde{\tilde{c}}_{ji} = \sqrt{2/(N+1)} \sin[\pi ji/(N+1)]$ [16–18], meaning that the expansion-coefficient matrix corresponds to the discrete sine-transformation matrix of type 1, denoted by $\mathbf{S}$. Matrix $\mathbf{S}$ is involutory, i.e., it is its own inverse, satisfying $\mathbf{S}^2 = \mathbf{I}$, where $\mathbf{I}$ is the identity matrix. Therefore, the single-waveguide modes can be expressed through the supermodes in exactly the same manner: $\bar{\mathbf{E}} = \mathbf{S}\tilde{\mathbf{E}}$. This relation has been used to calculate the field profiles in Fig. 1(b).

With the help of transformation matrix $\mathbf{S}$, the crosstalk of the waveguides in an array can be modeled analogously to optical diffraction in Fourier optics. Namely, given the initial complex amplitudes $\bar{\mathbf{a}}(0)$ of the modes in each waveguide, we obtain the supermode amplitudes from $\tilde{\mathbf{a}}(0)^T = \mathbf{S}\bar{\mathbf{a}}(0)^T$. Then, these amplitudes can be propagated using Eq. (3) and transformed back to the original

representation in terms of the amplitudes for the individual waveguides:

$$\bar{\mathbf{a}}(z)^T = \mathbf{S}\tilde{\mathbf{g}}(z)^T \circ \mathbf{S}\bar{\mathbf{a}}(0)^T. \tag{9}$$

We can eliminate the Hadamard product in Eq. (9) by turning the vector $\tilde{\mathbf{g}}$ into a diagonal matrix using operator $\mathrm{diag}(\cdot)$, which yields

$$\begin{aligned}\bar{\mathbf{a}}(z)^T &= \mathbf{S}\,\mathrm{diag}(\tilde{\mathbf{g}})\mathbf{S}\bar{\mathbf{a}}(0)^T \\ &= \bar{\mathbf{G}}(z)\bar{\mathbf{a}}(0)^T,\end{aligned} \tag{10}$$

where matrix

$$\bar{\mathbf{G}}(z) = \begin{bmatrix} \bar{g}_{11} & \bar{g}_{12} & \cdots & \bar{g}_{1N} \\ \bar{g}_{21} & \bar{g}_{22} & & \\ \vdots & & \ddots & \\ \bar{g}_{N1} & & & \bar{g}_{NN} \end{bmatrix} \tag{11}$$

has elements $\bar{g}_{ik} = \sum_{j=1}^{N} s_{ij} s_{kj} \exp(i\beta_j z)$ that are the weighted means of the propagational phase factors, with the weights determined by the products of the elements of $\mathbf{S}$. The elements $\bar{g}_{ik}$ describe the change in the complex amplitude of the mode in the ith waveguide due to the leakage from the kth waveguide. The matrix $\bar{\mathbf{G}}$ can be used to model the crosstalk in a concise manner. In Sec. III, we show that the approach can be generalized to include the treatment of bent waveguide arrays as well.

III. TRANSFORMATION MATRICES FOR A BENT WAVEGUIDE ARRAY

Consider an array of waveguides that are locally bent to form concentric rings (see Fig. 2). Let the mean radius of curvature of the array be R. The eigenmodes of this bent waveguide array, with the field distributions denoted by $\check{\mathbf{e}}$, are invariant with respect to the *angular* propagation along the φ coordinate rather than a linear propagation along z. Using the invariance, we choose $\check{\mathbf{e}} \propto \exp(i\alpha\varphi)\check{\mathbf{e}}(x,y)$ as an
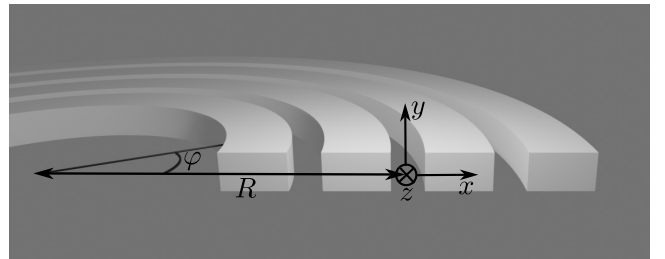

FIG. 2. A bent waveguide array. The average radius of curvature of the waveguides is R.

ansatz and write the Helmholtz equation in the form

$$\frac{\partial^2 \breve{\mathbf{e}}}{\partial x^2} + \frac{1}{x}\frac{\partial \breve{\mathbf{e}}}{\partial x} + \left(k^2 - \frac{\alpha^2}{x^2}\right)\breve{\mathbf{e}} + \frac{\partial^2 \breve{\mathbf{e}}}{\partial y^2} = 0, \quad (12)$$

which resembles the Bessel equation, except for the additional y-dependent term. Consequently, the fields in the waveguides can be expressed in terms of Bessel functions of the first and second kind as $\breve{e} \propto J_\alpha(k_x x) + Y_\alpha(k_x x)$ [22]. Here, α is the angular-propagation constant.

Our aim is to represent the bent-array supermodes $\breve{\mathbf{E}} = [\breve{e}_1 \ \breve{e}_2 \ \cdots \ \breve{e}_N]^T$ in terms of the corresponding straight-array supermodes $\tilde{\mathbf{E}}$. We start with an approach introduced in Ref. [20] and look for a set of expansion coefficients $\breve{\mathbf{c}}$ in the expansion of a single supermode of the bent waveguide array $\breve{e} = \breve{\mathbf{c}}\tilde{\mathbf{E}}$ that are invariant with respect to the field propagation over an infinitesimally small angular distance $d\varphi$. This approach is presented in Appendix A, where in contrast to Ref. [20], which considers a scalar field in a single waveguide, we consider a vector field in a waveguide array. We simplify the approach by assuming that only N supermodes comprise matrix $\tilde{\mathbf{E}}$, which, in general, makes the representation incomplete, as $\breve{e} \notin \text{span}(\tilde{\mathbf{E}})$. Strictly speaking, bending the waveguides can modify the mode profiles in the individual waveguides and lead to coupling of the modes to other propagating or leaky modes. However, these N supermodes have a dominant contribution to $\breve{e}$, resulting in a representation that is almost indistinguishable from the actual one, as will be demonstrated shortly.

In Appendix A, it is shown that vector $\breve{\mathbf{c}}$ satisfies

$$\breve{\mathbf{c}}\left[R\mathbf{I} + \mathbf{S}\,\text{diag}(\mathbf{x})\mathbf{S}\right]\text{diag}(\boldsymbol{\beta}) = \alpha\breve{\mathbf{c}}, \quad (13)$$

where the elements of vector $\mathbf{x} = \Lambda_x(\mathbf{i} - \langle i \rangle \mathbf{1})$ are the x coordinates at the center of each waveguide. Here, $\mathbf{i}$ and $\mathbf{1}$ are N-dimensional vectors, the first of which contains the waveguide indices, i.e., $\mathbf{i} = [1 \ 2 \ \cdots \ N]$, whereas the elements of the second one are all equal to 1. The matrix on the left-hand side of Eq. (13) can be simplified by expressing the propagation constants in terms of their deviation from the mean: $\boldsymbol{\beta} = \langle \beta \rangle \mathbf{1} + \Delta\boldsymbol{\beta}$, where $\langle \beta \rangle = \sum_{j=1}^{N}\beta_j/N$ is the average propagation constant. We then neglect the term $\mathbf{S}\text{diag}(\mathbf{x})\mathbf{S}\text{diag}(\Delta\boldsymbol{\beta})$, assuming that the elements of $\Delta\boldsymbol{\beta}$ are all small compared to $\langle \beta \rangle$. Note also that the largest element of $\mathbf{x}$ is smaller than R, because the half width of the array is smaller than R. This leaves us with a matrix

$$\mathbf{M} = R\langle \beta \rangle \mathbf{I} + R\,\text{diag}(\Delta\boldsymbol{\beta}) + \langle \beta \rangle \mathbf{S}\,\text{diag}(\mathbf{x})\mathbf{S} \quad (14)$$

and the following eigenproblem:

$$\breve{\mathbf{c}}\mathbf{M} = \alpha\breve{\mathbf{c}}. \quad (15)$$

The eigenvector $\breve{\mathbf{c}}$ as a solution of Eq. (15) contains the expansion coefficients of the representation and the

eigenvalue, α, is the angular-propagation constant that determines the phase $\phi = \alpha\varphi$ of the propagation-invariant eigenstate.

While it is possible to solve the eigenproblem directly for small number of waveguides — say, $N \leq 5$ — the resulting expressions for $N > 2$ are incomprehensible and do not give much insight into the behavior of the system. Therefore, before attempting to solve the problem for such cases, several observations are made regarding matrix $\mathbf{M}$. We start by introducing vector $\boldsymbol{\rho} = [\rho_1 \ \rho_2 \ \cdots \ \rho_N]$, with elements

$$\rho_j = \frac{R\Delta\beta_j}{\Lambda_x \langle \beta \rangle}, \quad (16)$$

which can be used to rewrite $\mathbf{M}$ as

$$\mathbf{M} = \langle \beta \rangle \left[R_0\mathbf{I} + \Lambda_x\left(\text{diag}(\boldsymbol{\rho}) + \mathbf{S}\,\text{diag}(\mathbf{i})\mathbf{S}\right)\right], \quad (17)$$

where the constant $R_0 = R - \Lambda_x \langle i \rangle$ has been introduced to shorten the expressions. Let us also note that matrix $\mathbf{M}$ has the eigendecomposition $\mathbf{M} = \breve{\mathbf{C}}^{-1}\text{diag}(\boldsymbol{\alpha})\breve{\mathbf{C}}$, where matrix $\breve{\mathbf{C}}$ is composed of eigenvectors $\breve{\mathbf{c}}$ and vector $\boldsymbol{\alpha}$ contains the eigenvalues. Hence, matrix $\mathbf{M}$ can be diagonalized, using the expression

$$\begin{aligned}\text{diag}(\boldsymbol{\alpha}) &= \breve{\mathbf{C}}\mathbf{M}\breve{\mathbf{C}}^{-1} \\ &= \langle \beta \rangle \left[R_0\mathbf{I} + \Lambda_x\breve{\mathbf{C}}\left(\text{diag}(\boldsymbol{\rho}) + \mathbf{S}\,\text{diag}(\mathbf{i})\mathbf{S}\right)\breve{\mathbf{C}}^{-1}\right]\end{aligned} \quad (18)$$

to show that matrix $\breve{\mathbf{C}}$ also diagonalizes the matrix

$$\boldsymbol{\Gamma}(\boldsymbol{\rho}) = \text{diag}(\boldsymbol{\rho}) + \mathbf{S}\,\text{diag}(\mathbf{i})\mathbf{S}. \quad (19)$$

Therefore, the eigenvectors of $\mathbf{M}$ are equivalent to the eigenvectors of $\boldsymbol{\Gamma}$ and, as such, they are determined solely by $\boldsymbol{\rho}$. Furthermore, the angular-propagation constants can be expressed in the form

$$\boldsymbol{\alpha} = \langle \beta \rangle \left[R_0\mathbf{1} + \Lambda_x\boldsymbol{\gamma}(\boldsymbol{\rho})\right], \quad (20)$$

where the elements of $\boldsymbol{\gamma}$ are the eigenvalues of $\boldsymbol{\Gamma}$.

For large R, the second term in Eq. (19) can be neglected and one obtains $\breve{\mathbf{C}} \approx \mathbf{I}$ and $\breve{\mathbf{E}} \approx \tilde{\mathbf{E}}$, which means that the bent-array modes look like the supermodes of the corresponding straight array. Obviously, this has to be the case, since increasing the radius of curvature makes the waveguide array straighter. The corresponding angular-propagation constants are $\boldsymbol{\alpha} \approx R\boldsymbol{\beta}$, because $\boldsymbol{\gamma} \approx \boldsymbol{\rho}$. If, on the other hand, the radius of the array R is small, we obtain $\boldsymbol{\Gamma} \approx \mathbf{S}\,\text{diag}(\mathbf{i})\mathbf{S}$, from which it follows that $\breve{\mathbf{C}} \approx \mathbf{S}$ and $\breve{\mathbf{E}} \approx \bar{\mathbf{E}}$. This result implies that the eigenmodes of a

significantly bent waveguide array look like the modes of the individual waveguides that compose the array. This corresponds to full crosstalk suppression by bending. In this case, the angular-propagation constants are calculated from $\boldsymbol{\alpha} \approx \langle \beta \rangle \, \mathbf{R}$, since $\boldsymbol{\gamma} \approx \mathbf{i}$. The elements of $\mathbf{R} = R\mathbf{1} + \mathbf{x}$ are the radii of curvature at the center of each individual waveguide.

The crosstalk suppression by bending can be understood by comparing a bent waveguide array to a superlattice array [32,35], where the coupling between neighboring waveguides is suppressed by a propagation-constant mismatch due to different core sizes [37]. For a bent waveguide array, the crosstalk suppression is achieved due to a mismatch in the *angular* propagation constants and the corresponding angular phase velocities. The angular phase velocity of an eigenmode of a bent waveguide array (with one or more waveguides) is

$$v_\alpha = \frac{d\varphi}{dt} = \frac{\omega}{\alpha}, \tag{21}$$

where ω is the mode frequency. Since α is proportional to the radius of curvature of the waveguide, the angular phase velocity is inversely proportional to this radius. In contrast, the linear phase velocity ω/β is the same for all individual waveguides in the array. Therefore, it takes different times for light to propagate through the bent section of the array via different waveguides. This prevents the light in two different waveguides from contributing to the same eigenmode of a bent waveguide array, leading to crosstalk suppression.

One can also note that the propagation constants of the supermodes of a straight waveguide array satisfy $\Delta\beta_j \propto \cos[\pi j /(N + 1)]$ [16–18]. This, however, is the case only for the fundamental modes of the waveguides. The propagation constants of higher-order modes do not follow this simple pattern [26]. For fundamental modes, vector $\boldsymbol{\rho}$ can be rewritten by using the supermode index vector $\mathbf{j} = [1 \ 2 \ \cdots \ N]$ and a scalar parameter

$$\rho = \frac{R \max(\boldsymbol{\Delta\beta})}{\Lambda_x \langle \beta \rangle \cos[\pi/(N + 1)]} \tag{22}$$

to obtain

$$\boldsymbol{\rho} = \rho \cos \frac{\pi \mathbf{j}}{N + 1}. \tag{23}$$

Consequently, matrix $\boldsymbol{\Gamma}$ (which describes a bent waveguide array) appears to be determined solely by the scalar ρ, in accordance with the expression

$$\boldsymbol{\Gamma}(\rho) = \mathbf{S} \left[\frac{\rho}{2} \mathbb{I} + \operatorname{diag}(\mathbf{i}) \right] \mathbf{S}, \tag{24}$$

where

$$\mathbb{I} = 2\mathbf{S} \, \operatorname{diag}\left(\cos \frac{\pi \mathbf{j}}{N + 1} \right) \mathbf{S} = \begin{bmatrix} 0 & 1 & & & \\ 1 & 0 & 1 & & \\ & 1 & 0 & \ddots & \\ & & \ddots & \ddots & \end{bmatrix}. \tag{25}$$

In the above matrix, all the elements that are not addressed are equal to 0. We see that the expansion-coefficient matrix $\check{\mathbf{C}}(\rho)$ of a bent waveguide array, and hence the crosstalk suppression, can be assessed by evaluating the dimensionless radius of curvature ρ.

With the matrix given in Eq. (24), we can finally tackle the eigenproblem. For an array of two waveguides, the angular-propagation constants form the vector

$$\begin{aligned} \boldsymbol{\alpha} &= \langle \beta \rangle \left(R\mathbf{1} + \mathbf{x}\sqrt{1 + \rho^2} \right) \\ &= R \left(\langle \beta \rangle \, \mathbf{1} + \boldsymbol{\Delta\beta}\sqrt{1 + \rho^{-2}} \right), \end{aligned} \tag{26}$$

which, at small and large ρ, behaves as described above for the cases of small and large R. The corresponding eigenvectors are given in the matrix

$$\check{\mathbf{C}} = \mathcal{N} \begin{bmatrix} -\rho + \sqrt{1 + \rho^2} & 1 \\ -\rho - \sqrt{1 + \rho^2} & 1 \end{bmatrix}, \tag{27}$$

where a diagonal matrix

$$\mathcal{N} = \operatorname{diag}\left(\begin{bmatrix} \left[1 + \left(\rho - \sqrt{1 + \rho^2} \right)^2 \right]^{-1/2} \\ \left[1 + \left(\rho + \sqrt{1 + \rho^2} \right)^2 \right]^{-1/2} \end{bmatrix} \right) \tag{28}$$

takes care of the normalization of eigenvectors, $\|\check{\mathbf{c}}\| = 1$. The matrix given in Eq. (27) allows us to represent the supermodes of a bent waveguide array, incorporated in $\check{\mathbf{E}}$, in terms of the supermodes of the corresponding straight waveguide array, appearing in $\tilde{\mathbf{E}}$, while the inverse transform is given by $\check{\mathbf{C}}^{-1} = \check{\mathbf{C}}$. It is worth recalling that the solutions to eigenproblems are determined up to an arbitrary phase factor $\exp(i\phi)$. Now, to find a transformation between the supermodes of the bent waveguide array and the fields in the individual waveguides, i.e., between $\check{\mathbf{E}}$ and $\bar{\mathbf{E}}$, we simply combine the transformations $\tilde{\mathbf{E}} = \mathbf{S}\bar{\mathbf{E}}$ and

$\check{\mathbf{E}} = \check{\bar{\mathbf{C}}}\tilde{\mathbf{E}}$. This gives $\check{\mathbf{E}} = \check{\bar{\mathbf{C}}}\bar{\mathbf{E}}$, with

$$\check{\bar{\mathbf{C}}} = \check{\mathbf{C}}\mathbf{S}$$
$$= \frac{\mathcal{N}}{\sqrt{2}}\begin{bmatrix} 1 - \rho + \sqrt{1+\rho^2} & -1 - \rho + \sqrt{1+\rho^2} \\ 1 - \rho - \sqrt{1+\rho^2} & -1 - \rho - \sqrt{1+\rho^2} \end{bmatrix}$$
$$(29)$$

being the transformation matrix for an array of two waveguides.

For an array consisting of three waveguides, the solution to the eigenproblem is given in Appendix B. However, for larger arrays ($N > 3$), the expressions accompanying the solution of the eigenproblem are too cumbersome to deal with. Therefore, it is more insightful to look for the solutions graphically. As an example, consider an array of 15 waveguides. The expansion coefficients, i.e., the elements of matrix $\check{\bar{\mathbf{C}}}(\rho)$, for the representation of the bent-array supermodes as superpositions of the modes of individual waveguides are shown in Fig. 3(a) for various values of ρ between 0 and 500. The expansion coefficients enter
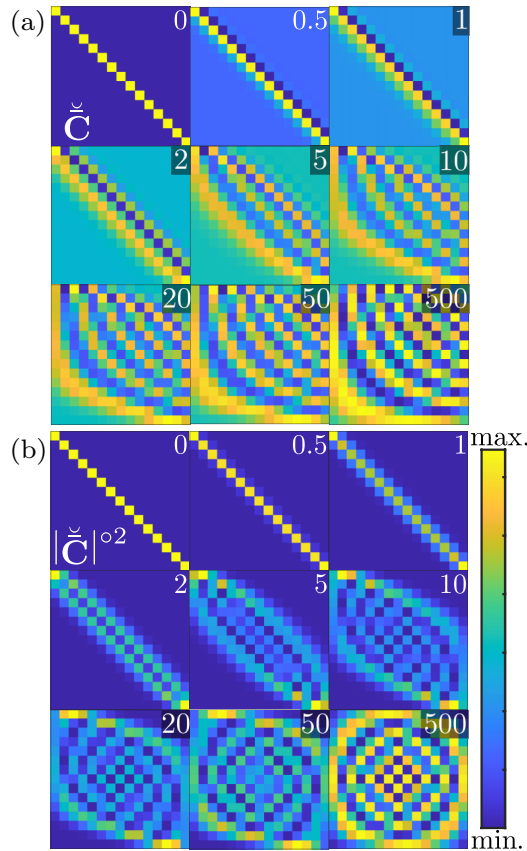

FIG. 3. (a) The normalized elements of the mode-expansion matrix $\check{\bar{\mathbf{C}}}$ for an array of 15 waveguides with $\rho = \{0, 0.5, 1, 2, 5, 10, 20, 50, 500\}$. (b) The corresponding normalized elements of $|\check{\bar{\mathbf{C}}}|^{\circ 2}$.

the amplitudes of the fields and the optical powers in the modes are proportional to the elements of $|\check{\bar{\mathbf{C}}}|^{\circ 2} = \check{\bar{\mathbf{C}}}^* \circ \check{\bar{\mathbf{C}}}$. These elements are shown in Fig. 3(b). From Fig. 3, it can be seen that, for $\rho < 1$, the power of the ith supermode is mostly confined to the ith waveguide, with a small portion leaked to the neighboring waveguides. For $\rho = 2$, the supermode is no longer confined in the same waveguide but spreads considerably to the two neighboring waveguides. It spreads further to the other waveguides in the array as ρ increases. For $\rho = 500$, $\check{\bar{\mathbf{C}}}$ is practically indistinguishable from $\mathbf{S}$, except for the different permutations of the eigenvectors. Here, we have $\alpha_1 < \alpha_2 < \cdots$, whereas $\beta_1 > \beta_2 > \cdots$ for the linear propagation constants. The chosen order of eigenvectors and eigenvalues is considered the most convenient, as it satisfies $\check{\bar{\mathbf{C}}}(0) = \mathbf{I}$. Note also that matrix $\check{\bar{\mathbf{C}}}$ is orthonormal, i.e., $\check{\bar{\mathbf{C}}} = \check{\bar{\mathbf{C}}}^{-1} = \check{\bar{\mathbf{C}}}^T$, which means that the elements of the ith column of $|\check{\bar{\mathbf{C}}}|^{\circ 2}$ show the relative powers of supermodes excited by light entering the bent section of the waveguide array via the ith waveguide.

The eigenvalues $\gamma_j(\rho)$ as functions of ρ for the array of 15 waveguides are shown in Fig. 4. For $\rho < 2$, the eigenvalues appear to satisfy the previously considered approximation $\boldsymbol{\gamma} \approx \mathbf{i}$. If ρ increases, the eigenvalues fan out. Crucially, the separation of the eigenvalues, $\gamma_{j+1} - \gamma_j$, starts to depend on j. This has a major consequence on the crosstalk dynamics, as will be shown in Sec. IV.

The accuracy of the derived representations can be verified by numerically calculating $\check{\mathbf{E}}$ and $\boldsymbol{\alpha}$ for a bent waveguide array, as well as $\tilde{\mathbf{E}}$ and $\boldsymbol{\beta}$ for a straight array. The supermodes of a bent waveguide array can be obtained numerically using an eigenvalue solver in cylindrical coordinates (the 2D axisymmetric space dimension in COMSOL MULTIPHYSICS). The calculated propagation constants of the supermodes, forming vector $\boldsymbol{\beta}$, and the values of Λ_x and R are used to calculate the dimensionless radius ρ, eigenvalues $\boldsymbol{\gamma}$, and mode-expansion matrices $\check{\bar{\mathbf{C}}}$. The eigenvalues $\boldsymbol{\gamma}$ are then used to calculate the 2-norm error
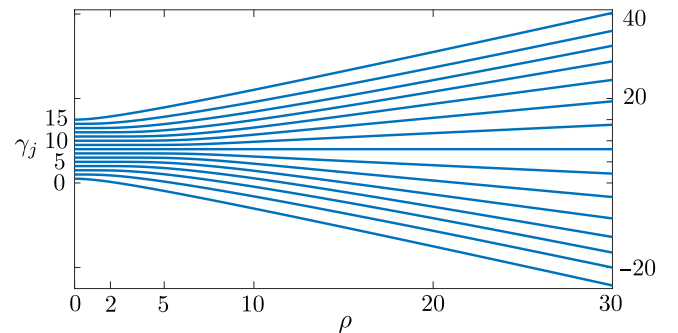

FIG. 4. The eigenvalues γ_j for an array of 15 waveguides with $\rho \in [0, 30]$.

in the estimation of the angular-propagation constant:

$$\epsilon_\alpha = \frac{\|\mathrm{Re}\{\boldsymbol{\alpha}\} - \langle\beta\rangle\,(R_0\mathbf{1} + \Lambda_x\boldsymbol{\gamma})\|}{\|\mathrm{Re}\{\boldsymbol{\alpha}\}\|}, \qquad (30)$$

whereas matrices $\breve{\check{\mathbf{C}}}$ are used to obtain the representations $\breve{\mathbf{E}} = \breve{\check{\mathbf{C}}}\tilde{\mathbf{E}}$ (minding the relative phases and the permutation of the supermodes). We start by calculating the TE modes for bent waveguide arrays with the radial cross section identical to the transverse cross section of a straight waveguide in Fig. 1. The radii of curvature R have been chosen to be 2, 210, and 2100 µm to obtain, respectively, the values of ρ equal to 0.005, 0.5, and 5. The resulting electric field distributions of the modes are shown in Figs. 5(a)–5(f), respectively. The numerically calculated mode profiles are shown in Figs. 5(a), 5(c), and 5(f), and the profiles in Figs. 5(b), 5(d), and 5(f) are obtained from the representations $\breve{\check{\mathbf{C}}}\tilde{\mathbf{E}}$. The latter are practically indistinguishable from the former, showing a high accuracy of our analytical approach. Likewise, the estimated real part of the angular-propagation constant is, in all the cases considered, equal to its actual values, as indicated by negligibly small errors $\epsilon_\alpha = \{4 \times 10^{-3}, 1 \times 10^{-5}, 8 \times 10^{-7}\}$ corresponding to Figs. 5(a)–5(f), respectively. However, the supermode $\breve{\mathbf{e}}_1$ shown in Fig. 5(a) has a noticeable attenuation, $\mathrm{Im}\{\alpha_1\} \approx -0.01$, which our model fails to capture. This follows from representing the bent-array supermodes using their straight-array counterparts, while neglecting the
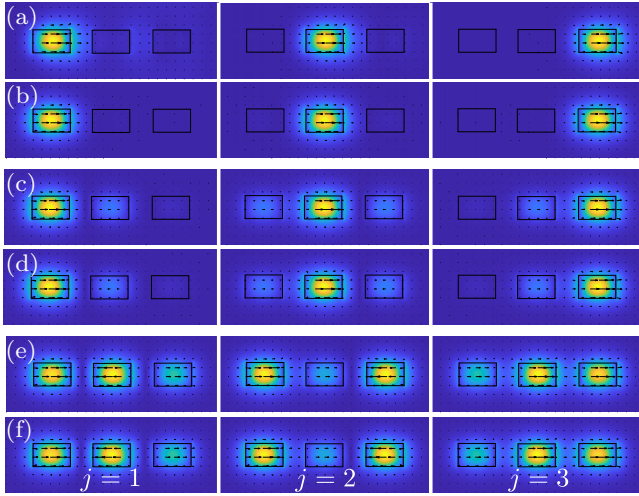
contributions from leaky modes that can appear due to bending.

To show that our theory is also applicable to other types of modes and waveguide arrays, we consider three more examples (see Fig. 6). In the first example, shown in Figs. 6(a) and 6(b), the waveguides are separated by a larger distance, such that $\Lambda_x = 1000$ nm. In the second example, shown in Figs. 6(c) and 6(d), the transverse-magnetic (TM) modes are considered. In the third example, shown in Figs. 6(e) and 6(f), the structure is replaced with a rib waveguide array consisting of a 200-nm-high silicon slab with 100×300 nm^2 strips on a glass substrate surrounded by air. The dimensionless radius ρ in these examples is equal to 0.5. It can be seen that the numerically found supermodes [Figs. 6(a), 6(c), and 6(e)] are essentially identical to the supermodes corresponding to our representation $\breve{\check{\mathbf{C}}}\tilde{\mathbf{E}}$ [Figs. 6(b), 6(d), and 6(f)]. While the parameter ρ is the same in these examples, the actual radii of curvature R are different, being equal to 1.8 mm, 45 µm, and 30 µm for the examples in Figs. 6(a)–6(f), respectively. This reflects the difference in the crosstalk for the corresponding straight waveguide arrays. In fact, the higher-order modes, for which the elements of $\Delta\boldsymbol{\beta}$ are much smaller than for the fundamental modes [26], could possess notable crosstalk suppression for much larger radii of curvature. For the supermodes shown in Figs. 6(a)–6(d), the estimates for the angular-propagation constant have the respective errors $\epsilon_\alpha = 8 \times 10^{-7}$ and $\epsilon_\alpha = 3 \times 10^{-5}$, which are negligibly small. In fact, for the rib waveguide
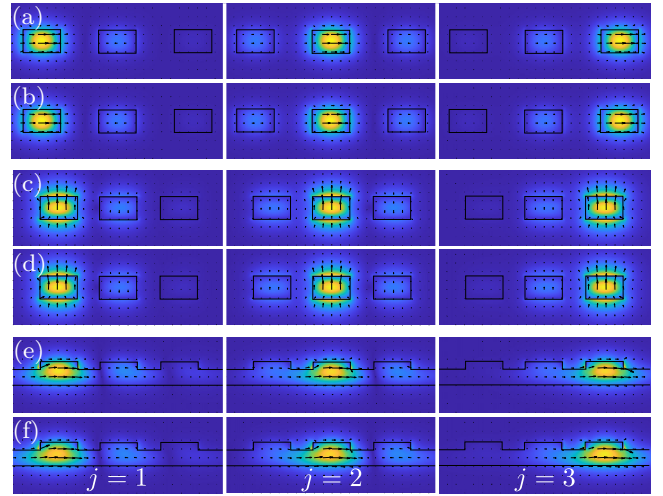

FIG. 5. The field distributions of supermodes $\breve{\mathbf{e}}_j$ of a bent waveguide array. The actual, numerically calculated, profiles are shown in (a), (c), and (e), while the corresponding profiles shown in (b), (d), and (f) are obtained as superpositions of the supermodes of a straight waveguide array. The bent waveguide arrays are obtained by bending the array of Fig. 1 such that the radius of curvature R is equal to 2, 210, and 2100 µm in (a),(b), (c),(d), and (e),(f), respectively.

FIG. 6. The (a),(c),(e) field distributions of supermodes $\breve{\mathbf{e}}_j$ of a bent waveguide array and (b),(d),(f) their representations as superpositions of the supermodes of the corresponding straight waveguide array. The waveguide arrays are bent such that $\rho = 0.5$. The array in (a)–(d) is similar to the array in Fig. 1, but in (a) and (b) the period is increased to $\Lambda_x = 1000$ nm. In (c) and (d), the transverse-magnetic (TM) modes are considered. In (e) and (f), the array is composed of rib waveguides.

array shown in Figs. 6(e) and 6(f), the error is larger, $\epsilon_\alpha = 6 \times 10^{-2}$, but still reasonably small. Hence, the representations appear to be very accurate and able to model the crosstalk dynamics for a variety of waveguide arrays.

IV. CROSSTALK DYNAMICS IN BENT WAVEGUIDE ARRAYS

With the expansion matrix $\breve{\mathbf{C}}$ and its inverse $\bar{\breve{\mathbf{C}}} = \breve{\mathbf{C}}^T$ introduced in Sec. III, Eq. (9) describing the propagation-related changes of the mode amplitudes in individual waveguides can be generalized to also treat bent waveguide arrays:

$$
\begin{aligned}
\bar{\mathbf{a}}(\varphi)^T &= \breve{\mathbf{C}}^T \operatorname{diag}(\breve{\mathbf{g}}(\varphi))\breve{\mathbf{C}}\bar{\mathbf{a}}(0)^T \\
&= \bar{\mathbf{G}}(\varphi)\bar{\mathbf{a}}(0)^T,
\end{aligned}
\tag{31}
$$

where

$$
\bar{\mathbf{G}}(\varphi) = \begin{bmatrix}
\bar{g}_{11} & \bar{g}_{12} & \cdots & \bar{g}_{1N} \\
\bar{g}_{21} & \bar{g}_{22} & & \\
\vdots & & \ddots & \\
\bar{g}_{N1} & & & \bar{g}_{NN}
\end{bmatrix}.
\tag{32}
$$

Analogous to the elements of matrix $\bar{\mathbf{G}}(z)$ in Eq. (11), the elements of $\bar{\mathbf{G}}(\varphi)$ describe the change in the complex amplitudes due to the crosstalk and are given by the following weighted means:

$$
\bar{g}_{ik} = \sum_{j=1}^{N} \bar{\breve{c}}_{ij}\bar{\breve{c}}_{kj}\exp(i\alpha_j\varphi).
\tag{33}
$$

Notably, for $\rho \gg N$, the elements of the straight waveguide array can be recovered, since we have

$$
\bar{g}_{ik} \approx \sum_{j=1}^{N} s_{ij}s_{kj}\exp(i\beta_j R\varphi)
\tag{34}
$$

for appropriately permuted eigenvectors and eigenvalues.

When it comes to the crosstalk, it is more insightful to consider the power exchange between the waveguides described by matrix

$$
|\bar{\mathbf{G}}(\varphi)|^{\circ 2} = \begin{bmatrix}
p_{11} & p_{12} & \cdots & p_{1N} \\
p_{21} & p_{22} & & \\
\vdots & & \ddots & \\
p_{N1} & & & p_{NN}
\end{bmatrix},
\tag{35}
$$

the elements of which are responsible for mode beating. These elements are (cf. Ref. [40])

$$
\begin{aligned}
p_{ik}(\varphi) =& \sum_{j=1}^{N} \bar{\breve{c}}_{ij}^2\bar{\breve{c}}_{kj}^2 \\
&+ 2\sum_{n>m} \bar{\breve{c}}_{in}\bar{\breve{c}}_{kn}\bar{\breve{c}}_{im}\bar{\breve{c}}_{km}\cos\left(\langle\beta\rangle\,\Lambda_x|\gamma_n - \gamma_m|\varphi\right),
\end{aligned}
\tag{36}
$$

where the fact that $|\alpha_n - \alpha_m| = \langle\beta\rangle\,\Lambda_x|\gamma_n - \gamma_m|$ has been used. In general, the crosstalk due to beating of more than two modes is a rather complicated phenomenon. However, its analysis is simplified when considering waveguide arrays with small ρ.

If ρ is sufficiently small, two simplifications can be done. One of them uses the fact that $\boldsymbol{\gamma} \approx \mathbf{i}$ and hence $|\gamma_n - \gamma_m| \approx |n - m|$, resulting in beat periods of $2\pi/(\langle\beta\rangle\,\Lambda_x|n - m|)$ for pairs of supermodes. The other simplification is based on the fact that the power of the ith supermode is mostly confined in the ith waveguide and can leak only to the immediate neighbors of this waveguide ($|\bar{\breve{c}}_{ii}| \gg |\bar{\breve{c}}_{ii\pm1}| \approx |\bar{\breve{c}}_{ii\pm1i}| \gg |\bar{\breve{c}}_{ii\pm2}| \cdots$). In such a case, almost all of the terms in Eq. (36) can be neglected. With these simplifications, the diagonal elements of $|\bar{\mathbf{G}}(\varphi)|^{\circ 2}$ are

$$
p_{ii}(\varphi) = \bar{\breve{c}}_{ii}^2\left[\bar{\breve{c}}_{ii}^2 + 2\left(\bar{\breve{c}}_{ii-1}^2 + \bar{\breve{c}}_{ii+1}^2\right)\cos\langle\beta\rangle\,\Lambda_x\varphi\right]
\tag{37}
$$

for $1 < i < N$, i.e., for waveguides that are not at the edge of the array. For the first and last waveguides, we obtain

$$
p_{ii}(\varphi) = \bar{\breve{c}}_{ii}^2\left[\bar{\breve{c}}_{ii}^2 + 2\bar{\breve{c}}_{ii\pm1}^2\cos\langle\beta\rangle\,\Lambda_x\varphi\right].
\tag{38}
$$

Equations (37) and (38) describe the propagation of light in the ith waveguide. The light power oscillates as a function of φ, with a period of $2\pi/\langle\beta\rangle\,\Lambda_x$. The power in the neighboring waveguides oscillates in accordance with

$$
p_{ii\pm1}(\varphi) = 4\bar{\breve{c}}_{ii}^2\bar{\breve{c}}_{i\pm1i}^2\sin^2\frac{\langle\beta\rangle\,\Lambda_x}{2}\varphi,
\tag{39}
$$

where it is assumed that $\bar{\breve{c}}_{ii\pm1} = -\bar{\breve{c}}_{i\pm1i}$, as dictated by symmetry (see also Fig. 3). These results show that the crosstalk can be minimized simply by making the angular-propagation distance equal to an integer multiple of $2\pi/\langle\beta\rangle\,\Lambda_x$.

As an example, in Fig. 7 we show the oscillation of optical power originally coupled to the first and fifth waveguides in an array of ten waveguides. The waveguides and their separation are the same as in Fig. 1. The radius of curvature of the array is set to 112.5 µm ($\rho = 0.25$), resulting in Fig. 7(a), and 225 µm ($\rho = 0.5$), resulting in Fig. 7(b). The normalized powers p_{11}, p_{55}, p_{12}, and p_{56} calculated using the exact Eq. (36) and the approximate
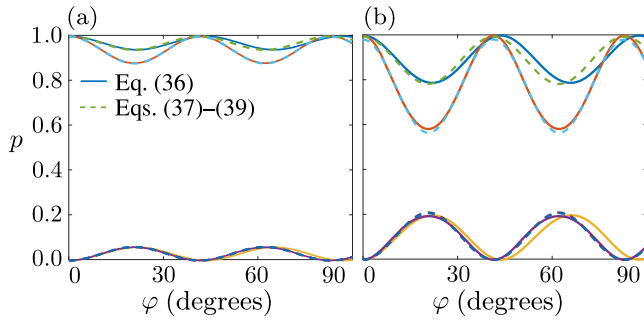
FIG. 7. The propagation of light originally confined in the first and fifth waveguides of bent arrays of ten waveguides with the radii of curvature of (a) 112.5 μm and (b) 225 μm. The exact expression for the power in the two waveguides and their neighbors ($i = 2$ and $i = 6$), given by Eq. (36) (solid lines), are compared to the approximate expressions, given by Eqs. (37)–(39) (dashed lines).

Eqs. (37)–(39) are shown by the solid and dashed curves, respectively, in Fig. 7. It can be seen that the approximate expressions are in good agreement with the exact one for both $\rho = 0.25$ [Fig. 7(a)] and $\rho = 0.5$ [Fig. 7(b)].

In order to visualize the phenomenon more clearly, we show in Fig. 8 how the power is distributed between the waveguides as a function of the propagation distance φR, for light originally coupled to [Fig. 8(a)] the first and [Fig. 8(b)] the fifth waveguide. The propagation distance is measured from the center of the array with radius of curvature $R = 225$ μm. However, the lengths of the neighboring waveguides in the bent section (spanning the angle of 180°) differ by $\Lambda_x \pi \approx 2.5$ μm. The first waveguide can be seen to periodically lose and gain less power than the fifth one (see Fig. 8), since it has only one neighboring waveguide.

For waveguide arrays with increasingly large ρ, light entering the bent section via a single waveguide excites an increasingly large number of supermodes (see the columns of $|\breve{\mathbf{C}}|^{\circ 2}$ in Fig. 3). Furthermore, the excited supermodes
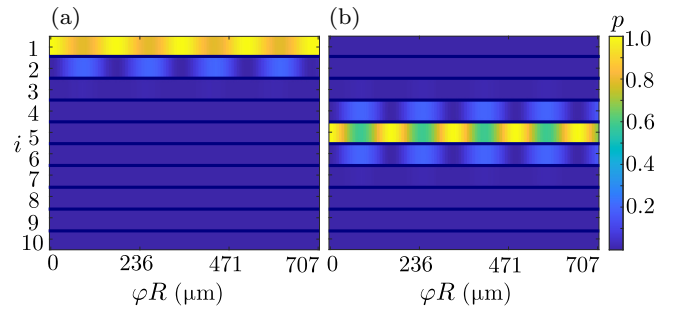

FIG. 8. The total power distribution as a function of the propagation distance for (a) the first and (b) the fifth waveguide of a bent array of ten waveguides with radius of curvature $R = 225$ μm.

allow the light to leak further away from the original waveguide (see the rows of $|\breve{\mathbf{C}}|^{\circ 2}$ in Fig. 3). This can be seen in Fig. 9, which shows the leakage of power from [Fig. 9(a)] the first and [Figs. 9(b)–9(d)] the fifth waveguide as a function of the propagation distance φR. The waveguide arrays are similar to the one in Fig. 8, except that the radius of curvature is increased to 450 μm in Figs. 9(a) and 9(b) and to 900 μm in Fig. 9(c). The array in Fig. 9(d) is straight. The bent arrays exhibit a periodic beating of the modes, even though the light spreads all over the array before returning back to the original waveguide. The spreading is especially pronounced in Fig. 9(c). Note that in straight arrays, light does not show this behavior, as also observed in Fig. 9(d). The periodic beating patterns observed in Fig. 9 are known as optical Bloch oscillations and are a consequence of the constant spacing of the propagation constants in the neighboring waveguides (the Wannier-Stark ladder) [38,39]. Light comes back to the original waveguide after propagating a distance that is equal to the lowest common multiple of the beating periods for all the pairs of the excited supermodes. As long as the eigenvalues γ_j are close to integers (see Fig. 4), the angular-beating period is $2\pi / \langle \beta \rangle \, \Lambda_x$, as is the case in
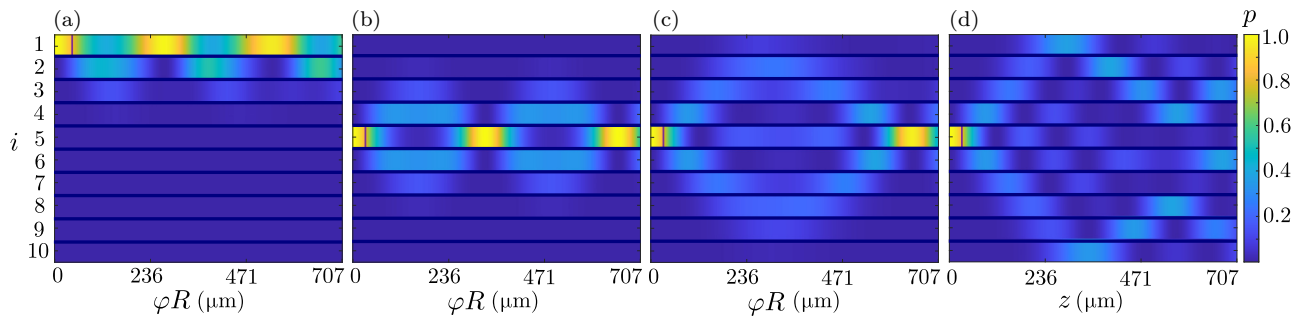

FIG. 9. The propagation of light originally confined in (a) the first and (b)–(d) the fifth waveguide of an array. The arrays in (a) and (b) are bent with the radii of curvature of 450 μm, whereas the array in (c) has a radius of 900 μm. The array in (c) is straight. The vertical purple lines show an estimate for a propagation distance after which 20% of light is lost from the original waveguide due to the crosstalk.

Figs. 9(b) and 9(c). However, at the edges of the array, the eigenvalues of the excited supermodes (see γ_1 and γ_N in Fig. 4) deviate from integer numbers for relatively small ρ when compared to the inner waveguides, shortening the beating period. This can be seen in Fig. 9(a). It should also be noted that while the angular-beating period $2\pi/\langle\beta\rangle\Lambda_x = 41°$ is same for the arrays in Figs. 8, 9(b), and 9(c), the linear-beating period $2\pi R/\langle\beta\rangle\Lambda_x$ increases with the radius of curvature R.

While it is possible to eliminate the crosstalk by matching the angular-propagation distance with the beat period, it is not always feasible. In such cases, it is more interesting to consider a limit for a propagation distance within which the crosstalk remains at an acceptable level. Note that for waveguide arrays with large radii of curvature, including straight ones, the beating period can be much longer than any practical propagation distance. Since even minor crosstalk can be detrimental to the performance of many devices, it is useful to consider the Taylor-series expansion of the power-exchange matrix:

$$|\bar{\mathbf{G}}(\varphi)|^{\circ2} = \mathbf{I} + \frac{d|\bar{\mathbf{G}}(0)|^{\circ2}}{d\varphi}\varphi + \frac{1}{2}\frac{d^2|\bar{\mathbf{G}}(0)|^{\circ2}}{d\varphi^2}\varphi^2, \quad (40)$$

where the series is truncated after the third term. We obtain the following expressions:

$$\frac{d|\bar{\mathbf{G}}(\varphi)|^{\circ2}}{d\varphi} = 2\left[\text{Re}\{\bar{\mathbf{G}}(\varphi)\} \circ \text{Re}\left\{\frac{d\bar{\mathbf{G}}(\varphi)}{d\varphi}\right\}\right.$$
$$\left. + \text{Im}\{\bar{\mathbf{G}}(\varphi)\} \circ \text{Im}\left\{\frac{d\bar{\mathbf{G}}(\varphi)}{d\varphi}\right\}\right], \quad (41)$$

$$\frac{d^2|\bar{\mathbf{G}}(\varphi)|^{\circ2}}{d\varphi^2} = 2\left[\text{Re}\left\{\frac{d\bar{\mathbf{G}}(\varphi)}{d\varphi}\right\}^{\circ2} + \text{Im}\left\{\frac{d\bar{\mathbf{G}}(\varphi)}{d\varphi}\right\}^{\circ2}\right.$$
$$+ \text{Re}\{\bar{\mathbf{G}}(\varphi)\} \circ \text{Re}\left\{\frac{d^2\bar{\mathbf{G}}(\varphi)}{d\varphi^2}\right\}$$
$$\left. + \text{Im}\{\bar{\mathbf{G}}(\varphi)\} \circ \text{Im}\left\{\frac{d^2\bar{\mathbf{G}}(\varphi)}{d\varphi^2}\right\}\right], \quad (42)$$

and

$$\frac{d^n\bar{\mathbf{G}}(0)}{d\varphi^n} = i^n\begin{bmatrix} \langle\alpha_j^n\rangle_{11} & \langle\alpha_j^n\rangle_{12} & \cdots & \langle\alpha_j^n\rangle_{1N} \\ \langle\alpha_j^n\rangle_{21} & \langle\alpha_j^n\rangle_{22} & & \\ \vdots & & \ddots & \\ \langle\alpha_j^n\rangle_{N1} & & & \langle\alpha_j^n\rangle_{NN} \end{bmatrix}, \quad (43)$$

where

$$\langle\alpha_j^n\rangle_{ik} = \sum_{j=1}^N \bar{\bar{c}}_{ij}\bar{\bar{c}}_{kj}\alpha_j^n. \quad (44)$$

The derivatives in Eq. (40) yield $d|\bar{\mathbf{G}}(0)|^{\circ2}/d\varphi = 0$ and

$$\frac{d^2|\bar{\mathbf{G}}(0)|^{\circ2}}{d\varphi^2} = -2\begin{bmatrix} \sigma_\alpha^2(1) & -\langle\alpha_j\rangle_{12}^2 & \cdots & -\langle\alpha_j\rangle_{1N}^2 \\ -\langle\alpha_j\rangle_{21}^2 & \sigma_\alpha^2(2) & & \\ \vdots & & \ddots & \\ -\langle\alpha_j\rangle_{N1}^2 & & & \sigma_\alpha^2(N) \end{bmatrix}, \quad (45)$$

where the diagonal elements of Eq. (45) correspond to the weighted variances of the angular-propagation constants

$$\sigma_\alpha^2(i) = \langle\alpha_j^2\rangle_{ii} - \langle\alpha_j\rangle_{ii}^2 = \sum_{j=1}^N \bar{\bar{c}}_{ij}^2\alpha_j^2 - \left(\sum_{j=1}^N \bar{\bar{c}}_{ij}^2\alpha_j\right)^2. \quad (46)$$

Hence, the Taylor expansion for the power-exchange matrix can be rewritten as

$$|\bar{\mathbf{G}}(\varphi)|^{\circ2}$$
$$= \mathbf{I} - \begin{bmatrix} \sigma_\alpha^2(1) & -\langle\alpha_j\rangle_{12}^2 & \cdots & -\langle\alpha_j\rangle_{1N}^2 \\ -\langle\alpha_j\rangle_{21}^2 & \sigma_\alpha^2(2) & & \\ \vdots & & \ddots & \\ -\langle\alpha_j\rangle_{N1}^2 & & & \sigma_\alpha^2(N) \end{bmatrix}\varphi^2, \quad (47)$$

where the diagonal elements, $1 - \sigma_\alpha^2(i)\varphi^2$, are the fractions of the light power left in the ith waveguide after propagation over angular distance φ. The fraction of the power escaping from the waveguide is therefore $F = \sigma_\alpha^2(i)\varphi^2$. If F is the allowed (small) loss level, the allowed angular-propagation distance is

$$\Phi_i(F) = \frac{\sqrt{F}}{\sigma_\alpha(i)}. \quad (48)$$

Evidently, the same treatment of the power-exchange matrix can also be done for a straight waveguide array, yielding the corresponding linear propagation distance

$$L_i(F) = \frac{\sqrt{F}}{\sigma_\beta(i)}, \quad (49)$$

where

$$\sigma_\beta^2(i) = \sum_{j=1}^N s_{ij}^2\beta_j^2 - \left(\sum_{j=1}^N s_{ij}^2\beta_j\right)^2. \quad (50)$$

Notably, for a directional coupler composed of two waveguides, we have $\sigma_\beta(i) \propto |\beta_1 - \beta_2| \; \forall i \in \{1,2\}$, meaning that

$L_i(F)$ is proportional to the coupling length. The propagation distances given by Eqs. (48) and (49) provide a good figure of merit when minimizing the crosstalk of waveguide arrays with large radii of curvature, including straight arrays. For numerical-computation purposes, it is worth mentioning that the weighted standard deviations calculated for all the waveguides can be collected to vector $\boldsymbol{\sigma_\alpha} = [\sigma_\alpha^2(1) \ \sigma_\alpha^2(2) \ \cdots \ \sigma_\alpha^2(N)]$ and evaluated simultaneously from the expression

$$\mathrm{diag}(\boldsymbol{\sigma_\alpha})^2 = \mathbf{I} \circ \left\{ \bar{\bar{\mathbf{C}}}\,\mathrm{diag}(\boldsymbol{\alpha})^2\check{\mathbf{C}} - \left[\bar{\bar{\mathbf{C}}}\,\mathrm{diag}(\boldsymbol{\alpha})\check{\mathbf{C}} \right]^{\circ 2} \right\}. \tag{51}$$

Likewise, for a straight waveguide array, we have

$$\mathrm{diag}(\boldsymbol{\sigma_\beta})^2 = \mathbf{I} \circ \left\{ \mathbf{S}\,\mathrm{diag}(\boldsymbol{\beta})^2\mathbf{S} - [\mathbf{S}\,\mathrm{diag}(\boldsymbol{\beta})\mathbf{S}]^{\circ 2} \right\}. \tag{52}$$

For the waveguide arrays shown in Fig. 9, the propagation distances after which 20% of the power is lost, calculated using Eqs. (48) and (49), are marked by the purple vertical lines. The propagation distances $\Phi_1(0.2) = 5.5°$, $\Phi_5(0.2) = 3.9°$, $\Phi_5(0.2) = 2°$, and $L_5(0.2) = 31$ µm in Figs. 9(a)–9(d), respectively, match the numerically evaluated power losses and thus validate Eqs. (48) and (49). Curiously, the linear propagation distances $\Phi_5(0.2)R$ in both Figs. 9(b) and 9(c) are approximately equal to that obtained for the straight waveguide array. This is because the initial loss of light is to the neighboring waveguides, which is not prevented by bending unless ρ is very small [see Fig. 5(a)]. Therefore, the crosstalk suppression is not guaranteed by bending but requires either a sufficiently small radius ρ or matching the angular size of the array to the angular-beating period $2\pi/\langle\beta\rangle\Lambda_x$.

V. CONCLUSIONS

In this work, an analytical method for modeling propagation of light in arrays of single-mode waveguides has been developed. The method can be applied to both bent and straight waveguide arrays. It is based on the decomposition of optical fields propagating in the array into its eigenmodes, here termed supermodes. We have demonstrated how the method can be used to characterize the crosstalk in an arbitrarily large waveguide array in a very efficient way that does not require computationally heavy three-dimensional simulations. We have found that, for bent waveguides, the crosstalk is characterized by a single scalar parameter ρ that is the dimensionless radius of curvature determined by the radius of curvature of the array and the phase mismatch between the modes. This can be used to assess the significance of the crosstalk without further calculations. The supermodes obtained by using our methods have been shown to be essentially indistinguishable from the modes obtained in rigorous numerical calculations. In combination with a discrete sine-transformation

matrix, $\mathbf{S}$, the transformation matrices introduced in this work to switch between different expansion bases have been shown to be especially effective for modeling the crosstalk dynamics. The expansion bases used are composed of modes of individual waveguides, supermodes of a straight waveguide array, and supermodes of a bent array. We have found that for bent waveguide arrays with small ρ, light confined in a single waveguide can only leak to the closest neighboring waveguides and that the leakage can be insignificant. This phenomenon can be used to suppress the crosstalk by bending the waveguides in the array. Additionally, we have shown that the crosstalk can exhibit a periodic beating pattern, which can also be used to minimize its influence on the output distribution of optical signals. The analysis presented provides an additional insight into the properties of light propagation in straight and bent waveguide arrays, as well as offering efficient computational tools that may be used to design densely packed waveguides with low crosstalk. The approach can be further developed toward arrays of waveguides carrying higher-order modes and possibly also three-dimensional waveguide arrays.

APPENDIX A: DERIVATION OF THE EIGENPROBLEM

Following the perturbation-based procedure introduced in Ref. [20], we suppose that the field of a supermode of a bent waveguide array can be represented in terms of the supermodes of the corresponding straight waveguide array by using the relation $\check{\mathbf{e}} = \check{\mathbf{c}}\tilde{\mathbf{E}}$. As an eigenmode, any element of $\check{\mathbf{e}}$ is invariant in its amplitude with respect to angular propagation. Propagation over an infinitesimal angular distance $d\varphi$ adds a phase to the field in accordance with

$$\begin{aligned}\check{\mathbf{e}}\exp(i\alpha\,d\varphi) &= \check{\mathbf{c}}\tilde{\mathbf{E}}\,\mathrm{diag}(\exp(i\boldsymbol{\beta}\,dz)) \\ \Rightarrow \check{\mathbf{e}}\alpha &= \check{\mathbf{c}}\tilde{\mathbf{E}}\,\mathrm{diag}(\boldsymbol{\beta}(R+x)),\end{aligned} \tag{A1}$$

where $dz(x) = (R+x)d\varphi$ is the corresponding change in the longitudinal coordinate z as a function of distance x from the center of the waveguide array with radius of curvature R (see Fig. 2). Here, the Taylor expansion is used to write the exponential function as $\exp\theta \approx 1-\theta$, for an infinitesimally small argument. Considering the propagated supermode $\check{\mathbf{e}}\alpha = \check{\mathbf{c}}\tilde{\mathbf{E}}\alpha$, we focus on the contribution to it of the jth supermode of the straight array, which can

be isolated by applying the overlap integral [see Eq. (5)] to Eq. (A1) for both the left- and right-hand sides, yielding

$$c(\tilde{\mathbf{e}}_j, \tilde{\mathbf{h}}_j, \breve{\mathbf{c}}\tilde{\mathbf{E}}\alpha, \breve{\mathbf{c}}\tilde{\mathbf{H}}\alpha) = \breve{c}_j \alpha \qquad (A2)$$

and

$$c(\tilde{\mathbf{e}}_j, \tilde{\mathbf{h}}_j, \breve{\mathbf{c}}\tilde{\mathbf{E}}\operatorname{diag}(\boldsymbol{\beta}(R+x)), \breve{\mathbf{c}}\tilde{\mathbf{H}}\operatorname{diag}(\boldsymbol{\beta}(R+x)))$$
$$= \breve{c}_j \beta_j R + \breve{\mathbf{c}}\operatorname{diag}(\boldsymbol{\beta})\mathbf{c}(\tilde{\mathbf{e}}_j, \tilde{\mathbf{h}}_j, x\tilde{\mathbf{E}}, x\tilde{\mathbf{H}}), \qquad (A3)$$

respectively, and using the orthonormality of the supermodes. In vector

$$\mathbf{c}(\tilde{\mathbf{e}}_j, \tilde{\mathbf{h}}_j, x\tilde{\mathbf{E}}, x\tilde{\mathbf{H}}) = \begin{bmatrix} c(\tilde{\mathbf{e}}_j, \tilde{\mathbf{h}}_j, x\tilde{\mathbf{e}}_1, x\tilde{\mathbf{h}}_1) \\ c(\tilde{\mathbf{e}}_j, \tilde{\mathbf{h}}_j, x\tilde{\mathbf{e}}_2, x\tilde{\mathbf{h}}_2) \\ \vdots \\ c(\tilde{\mathbf{e}}_j, \tilde{\mathbf{h}}_j, x\tilde{\mathbf{e}}_N, x\tilde{\mathbf{h}}_N) \end{bmatrix}, \qquad (A4)$$

the kth element can be found by representing the straight-array supermodes in terms of the single-waveguide modes:

$$c(\tilde{\mathbf{e}}_j, \tilde{\mathbf{h}}_j, x\tilde{\mathbf{e}}_k, x\tilde{\mathbf{h}}_k)$$
$$= \frac{1}{4} \iint_{-\infty}^{\infty} x \left(\tilde{\mathbf{e}}_j^* \times \tilde{\mathbf{h}}_k + \tilde{\mathbf{e}}_k \times \tilde{\mathbf{h}}_j^* \right) \cdot \hat{\mathbf{z}} \, dx \, dy$$
$$= \sum_{i=1}^{N} s_{ij} s_{ik} \frac{1}{2} \iint_{-\infty}^{\infty} x \operatorname{Re}\{\bar{\mathbf{e}}_i^* \times \bar{\mathbf{h}}_i\} \cdot \hat{\mathbf{z}} \, dx \, dy. \qquad (A5)$$

The integral in Eq. (A5) is recognized as the centroid of field $\bar{\mathbf{e}}_i$, i.e., the x coordinate at the center of the ith waveguide. Hence, we can write

$$c(\tilde{\mathbf{e}}_j, \tilde{\mathbf{h}}_j, x\tilde{\mathbf{e}}_k, x\tilde{\mathbf{h}}_k) = \sum_{i=1}^{N} s_{ij} s_{ik} x_i = \mathbf{s}_j \cdot \mathbf{x} \circ \mathbf{s}_k, \qquad (A6)$$

where the center coordinates are collected to the vector

$$\mathbf{x} = \Lambda_x (\mathbf{i} - \langle i \rangle \mathbf{1}). \qquad (A7)$$

Inserting the evaluated $\mathbf{c}(\tilde{\mathbf{e}}_j, \tilde{\mathbf{h}}_j, x\tilde{\mathbf{E}}, x\tilde{\mathbf{H}})$ into Eq. (A3) yields

$$\breve{c}_j \alpha = \breve{c}_j \beta_j R + \sum_{k=1}^{N} \sum_{i=1}^{N} \breve{c}_k \beta_k s_{ik} s_{ij} x_i. \qquad (A8)$$

Reconstructing the vector $\breve{\mathbf{c}}$ from the elements $\breve{c}_j$ that satisfy Eq. (A8), we obtain

$$\alpha\breve{\mathbf{c}} = \breve{\mathbf{c}}[R\mathbf{I} + \mathbf{S}\operatorname{diag}(\mathbf{x})\mathbf{S}]\operatorname{diag}(\boldsymbol{\beta}), \qquad (A9)$$

because

$$\breve{\mathbf{c}}\mathbf{S}\operatorname{diag}(\mathbf{x})\mathbf{S}\operatorname{diag}(\boldsymbol{\beta}) = \breve{\mathbf{c}}\mathbf{S} \begin{bmatrix} x_1\beta_1\mathbf{s}_1^T \\ x_2\beta_2\mathbf{s}_2^T \\ \vdots \\ x_N\beta_N\mathbf{s}_N^T \end{bmatrix}$$
$$= \begin{bmatrix} \sum_{k=1}^{N} \sum_{i=1}^{N} \breve{c}_k \beta_k s_{ik} s_{i1} x_i \\ \sum_{k=1}^{N} \sum_{i=1}^{N} \breve{c}_k \beta_k s_{ik} s_{i2} x_i \\ \vdots \\ \sum_{k=1}^{N} \sum_{i=1}^{N} \breve{c}_k \beta_k s_{ik} s_{iN} x_i \end{bmatrix}^T. \qquad (A10)$$

APPENDIX B: SOLUTION OF THE EIGENPROBLEM FOR ARRAYS THREE WAVEGUIDES

In the case of an array consisting of three waveguides, the eigenproblem has a solution with the angular-propagation constants forming the vector

$$\boldsymbol{\alpha} = \langle \beta \rangle \left(R\mathbf{1} + \mathbf{x}\sqrt{1 + \frac{\rho^2}{2}} \right)$$
$$= R \left(\langle \beta \rangle \mathbf{1} + \Delta\boldsymbol{\beta}\sqrt{1 + 2\rho^{-2}} \right) \qquad (B1)$$

and the expansion-coefficient matrix given by

$$\breve{\mathbf{C}} = \mathcal{N} \begin{bmatrix} 1 + \rho^2 - \rho\sqrt{2 + \rho^2} & -\rho + \sqrt{2 + \rho^2} & 1 \\ -1 & -\rho & 1 \\ 1 + \rho^2 + \rho\sqrt{2 + \rho^2} & -\rho - \sqrt{2 + \rho^2} & 1 \end{bmatrix}, \qquad (B2)$$

where the normalization matrix is

$$\mathcal{N} = \frac{1}{\sqrt{2 + \rho^2}} \operatorname{diag}\left(\begin{bmatrix} \left[2\left(1 + \rho^2 - \rho\sqrt{2 + \rho^2} \right) \right]^{-\frac{1}{2}} \\ 1 \\ \left[2\left(1 + \rho^2 + \rho\sqrt{2 + \rho^2} \right) \right]^{-\frac{1}{2}} \end{bmatrix} \right). \qquad (B3)$$

.

[1] D. Thomson, A. Zilkie, J. E. Bowers, T. Komljenovic, G. T. Reed, L. Vivien, D. Marris-Morini, E. Cassan, L. Virot, J.-M. Fédéli, J.-M. Hartmann, J. H. Schmid, D.-X. Xu, F. Boeuf, P. O'Brien, G. Z. Mashanovich, and M. Nedeljkovic, Roadmap on silicon photonics, J. Opt. **18**, 073003 (2016).

[2] W. Bogaerts and L. Chrostowski, Silicon photonics circuit design: Methods, tools and challenges, Laser Photonics Rev. **12,** 1700237 (2018).

[3] N. Margalit, C. Xiang, S. M. Bowers, A. Bjorlin, R. Blum, and J. E. Bowers, Perspective on the future of silicon photonics and electronics, Appl. Phys. Lett. **118,** 220501 (2021).

[4] S. Y. Siew, B. Li, F. Gao, H. Y. Zheng, W. Zhang, P. Guo, S. W. Xie, A. Song, B. Dong, L. W. Luo, C. Li, X. Luo, and G.-Q. Lo, Review of silicon photonics technology and platform development, J. Lightwave Technol. **39,** 4374 (2021).

[5] K. Okamoto, *Fundamentals of Optical Waveguides* (Elsevier Science & Technology, San Diego, 2006).

[6] D.-X. Xu, A. Densmore, A. Delâge, P. Waldron, R. McKinnon, S. Janz, J. Lapointe, G. Lopinski, T. Mischki, E. Post, P. Cheben, and J. H. Schmid, Folded cavity SOI microring sensors for high sensitivity and real time measurement of biomolecular binding, Opt. Express **16,** 15137 (2008).

[7] W.-C. Wang, W. R. Ledoux, C.-Y. Huang, C.-S. Huang, G. K. Klute, and P. G. Reinhall, Development of a microfabricated optical bend loss sensor for distributive pressure measurement, IEEE Trans. Biomed. Eng. **55,** 614 (2008).

[8] P. Munoz, D. Pastor, and J. Capmany, Modeling and design of arrayed waveguide gratings, J. Lightwave Technol. **20,** 661 (2002).

[9] X. J. M. Leijtens, B. Kuhlow, and M. K. Smit, in *Wavelength Filters in Fibre Optics*, Springer Series in Optical Sciences (Springer, Heidelberg, 2006), p. 125.

[10] P. McManamon, in *Liquid Crystals: Optics and Applications* (SPIE, Bellingham, 2005), Vol. 5947, p. 152.

[11] P. Dong, Silicon photonic integrated circuits for wavelength-division multiplexing applications, IEEE J. Sel. Top. Quantum Electron. **22,** 370 (2016).

[12] Y. Guo, Y. Guo, C. Li, H. Zhang, X. Zhou, and L. Zhang, Integrated optical phased arrays for beam forming and steering, Appl. Sci. **11,** 4017 (2021).

[13] M. J. R. Heck, Highly integrated optical phased arrays: Photonic integrated circuits for optical beam shaping and beam steering, Nanophotonics **6,** 93 (2017).

[14] H. Haus, W. Huang, S. Kawakami, and N. Whitaker, Coupled-mode theory of optical waveguides, J. Lightwave Technol. **5,** 16 (1987).

[15] W.-P. Huang, Coupled-mode theory for optical waveguides: An overview, J. Opt. Soc. Am. A **11,** 963 (1994).

[16] E. Kapon, J. Katz, and A. Yariv, Supermode analysis of phase-locked arrays of semiconductor lasers, Opt. Lett. **9,** 125 (1984).

[17] C. Xia, M. A. Eftekhar, R. A. Correa, J. E. Antonio-Lopez, A. Schülzgen, D. Christodoulides, and G. Li, Supermodes in coupled multi-core waveguide structures, IEEE J. Sel. Top. Quantum Electron. **22,** 196 (2016).

[18] M. L. Cooper and S. Mookherjea, Numerically-assisted coupled-mode theory for silicon waveguide couplers and arrayed waveguides, Opt. Express **17,** 1583 (2009).

[19] H. Deng, G. Jin, J. Harari, J. Vilcot, and D. Decoster, Investigation of 3D semivectorial finite-difference beam propagation method for bent waveguides, J. Lightwave Technol. **16,** 915 (1998).

[20] A. Melloni, F. Carniel, R. Costa, and M. Martinelli, Determination of bend mode characteristics in dielectric waveguides, J. Lightwave Technol. **19,** 571 (2001).

[21] D. Lenz, D. Erni, and W. Bächtold, Quasi-analytic formalism for mode characteristics in highly overmoded rectangular dielectric waveguide bends, J. Opt. Soc. Am. A **22,** 1968 (2005).

[22] K. R. Hiremath, M. Hammer, R. Stoffer, L. Prkna, and J. Čtyroký, Analytic approach to dielectric optical bent slab waveguides, Opt. Quantum Electron. **37,** 37 (2005).

[23] J. Huangfu, S. Xi, F. Kong, J. Zhang, H. Chen, D. Wang, B.-I. Wu, L. Ran, and J. A. Kong, Application of coordinate transformation in bent waveguides, J. Appl. Phys. **104,** 014502 (2008).

[24] W. Song, R. Gatdula, S. Abbaslou, M. Lu, A. Stein, W. Y.-C. Lai, J. Provine, R. F. W. Pease, D. N. Christodoulides, and W. Jiang, High-density waveguide superlattices with low crosstalk, Nat. Commun. **6,** 7027 (2015).

[25] B. Shen, R. Polson, and R. Menon, Increasing the density of passive photonic-integrated circuits via nanophotonic cloaking, Nat. Commun. **7,** 13126 (2016).

[26] S. Maurya, R. Kolkowski, M. Kaivola, and A. Shevchenko, Crosstalk reduction between closely spaced optical waveguides by using higher-order modes, Phys. Rev. Appl. **18,** 044077 (2022).

[27] X. Jiang, H. Wu, and D. Dai, Low-loss and low-crosstalk multimode waveguide bend on silicon, Opt. Express **26,** 17680 (2018).

[28] H.-K. Chiu, F.-L. Hsiao, C.-H. Chan, and C.-C. Chen, Compact and low-loss bent hollow waveguides with distributed Bragg reflector, Opt. Express **16,** 15069 (2008).

[29] D. Dai, Multimode optical waveguide enabling microbends with low inter-mode crosstalk for mode-multiplexed optical interconnects, Opt. Express **22,** 27524 (2014).

[30] M. F. Land, Compound eyes: Old and new optical mechanisms, Nature **287,** 681 (1980).

[31] A. Brückner, J. Duparré, F. Wippermann, P. Dannberg, and A. Bräuer, in *Flying Insects and Robots*, edited by D. Floreano, J.-C. Zufferey, M. V. Srinivasan, and C. Ellington (Springer-Verlag, Berlin, 2010), p. 127.

[32] H. Xu and Y. Shi, Ultra-broadband 16-channel mode division (de)multiplexer utilizing densely packed bent waveguide arrays, Opt. Lett. **41,** 4815 (2016).

[33] R. Gatdula, S. Abbaslou, M. Lu, A. Stein, and W. Jiang, Guiding light in bent waveguide superlattices with low crosstalk, Optica **6,** 585 (2019).

[34] X. Yi, H. Zeng, S. Gao, and C. Qiu, Design of an ultra-compact low-crosstalk sinusoidal silicon waveguide array for optical phased array, Opt. Express **28,** 37505 (2020).

[35] H. Zafar, B. Paredes, J. Villegas, M. Rasras, and M. F. Pereira, O-band TE- and TM-mode densely packed adiabatically bent waveguide arrays on the silicon-on-insulator platform, Opt. Express **31,** 21389 (2023).

[36] S. Longhi, Coherent destruction of tunneling in waveguide directional couplers, Phys. Rev. A **71,** 065801 (2005).

[37] N. Yang, H. Yang, H. Hu, R. Zhu, S. Chen, H. Zhang, and W. Jiang, Theory of high-density low-cross-talk waveguide superlattices, Photonics Res. **4,** 233 (2016).

[38] U. Peschel, T. Pertsch, and F. Lederer, Optical Bloch oscillations in waveguide arrays, Opt. Lett. **23,** 1701 (1998).

[39] R. Morandotti, U. Peschel, J. S. Aitchison, H. S. Eisenberg, and Y. Silberberg, Experimental observation of linear and nonlinear optical Bloch oscillations, Phys. Rev. Lett. **83,** 4756 (1999).

[40] P. Hildén, E. Ilina, M. Kaivola, and A. Shevchenko, Multifrequency Bessel beams with adjustable group velocity and longitudinal acceleration in free space, New. Phys. **24,** 033042 (2022).